Current-driven domain-wall dynamics in curved ferromagnetic nanowires

Benjamin Krüger and Daniela Pfannkuche
I. Institut für Theoretische Physik, Universität Hamburg, Jungiusstrasse 9, 20355 Hamburg, Germany

Markus Bolte, Guido Meier, and Ulrich Merkt
Institut für Angewandte Physik und Zentrum für Mikrostrukturforschung, Universität Hamburg, Jungiusstrasse 11, 20355 Hamburg, Germany

(Received 30 August 2006; revised manuscript received 30 November 2006; published 26 February 2007)

The current-induced motion of a domain wall in a semicircle nanowire with applied Zeeman field is investigated. Starting from a micromagnetic model we derive an analytical solution which characterizes the domain-wall motion as a harmonic oscillation. This solution relates the micromagnetic material parameters with the dynamical characteristics of a harmonic oscillator: i.e., domain-wall mass, resonance frequency, damping constant, and force acting on the wall. The time derivative of the current density greatly contributes to the force on the domain wall. For wires with strong curvature the dipole moment of the wall as well as its geometry influence the eigenmodes of the oscillator. Based on these results we suggest experiments for the determination of material parameters which otherwise are difficult to access. Numerical calculations confirm our analytical solution and show its limitations.

DOI: 10.1103/PhysRevB.75.054421 PACS number(s): 75.60.Ch, 72.25.Ba, 76.50.+g

I. INTRODUCTION

The field-driven dynamics of magnetic domain walls has been intensely studied over the last decades.[1,2] The topic has recently regained interest by the discovery that spin-polarized currents of high density can alter magnetization configurations[3–6] and move domain walls.[7–11] Current-induced magnetic switching is viewed as a promising solution for the realization of magnetic random access memories,[6,12,13] while current-induced domain-wall motion has potential applications in spintronic data storage devices: e.g., in the racetrack memory[14] or data transfer schemes.[15–17] Several models of current-driven magnetization dynamics have been established to explain the electronic origin of current-induced magnetization changes and to predict their effects.[3,4,18–21] At first it was assumed that for finite domain walls the spins of the conduction electrons adiabatically follow the local magnetic moments.[18,22] Later the theoretical model was extended to include a nonadiabatic mismatch between the polarization of the current and the direction of the magnetization.[19–21]

The measured and calculated velocities of current-driven magnetic domain walls in thin nanowires vary by several orders of magnitude even for the same material.[7,21,23–25] While it has been originally suggested that the discrepancy could be due to thermal activation[11,25–28] or surface roughness,[25] it has recently been found that the domain-wall velocity depends on the type of the domain wall[26,29] which can be changed by a spin-polarized current.[8,26,30,31] Recently it has been observed that the velocity of field-driven domain-wall motion[32] can be altered by ±100 m/s by a pulsed spin-polarized current[33] and that the motion can even be halted completely.[34] It is now assumed that the adiabatic term is largely responsible for the acceleration of the domain wall while the nonadiabatic term will cause the wall to continually move.[21]

In this paper we use an alternating current to excite transverse walls in thin narrow rings. From a micromagnetic description we derive a hitherto phenomenological harmonic oscillator model which well describes the wall motion in this geometry. Experimentally it has been shown that domain-wall oscillations excited with an alternating current at their resonance frequency require current densities one to two orders of magnitude less (10^{10} A/m^2; see Refs. 9 and 35) than for pulsed excitations (10^{11}–10^{12} A/m^2; see Refs. 6, 7, 11, and 26). Our calculations show that the time derivative of the current density greatly contributes to the force on the domain wall which could be an explanation for this phenomenon. Experimentally alternating current excitation is advantageous because it allows for time-resolved imaging of the domain-wall motion by its periodic return to the initial state.

This work is organized in two parts presenting an analytical model for the description of domain walls in curved nanowires and a numerical investigation supporting the analytical model as well as showing its limitations. The analytical model used to describe the motion of a domain wall in a nanowire is developed in the framework of the one-dimensional (1D) approximation as done previously for field-driven motion[36] and direct-current-driven spin torque.[21,25,34] We here limit ourselves to the spin-transfer torque. This approach is valid to describe ferromagnetic metals where the Fermi wavelength is much smaller than the size of the magnet and the width of the domain wall.[18] Solving analytically the Landau-Lifshitz-Gilbert equation extended by the current corrections due to Zhang and Li[21] we are able to express the properties of the driven oscillator by the quantities determining the micromagnetic model. Furthermore, we are able to include the influence of alternating current excitation, i.e., the time derivative of the current density. A comparison of the numerical calculations with our analytical solution confirms the importance of the geometry due to the curved wires. Finally, we suggest experiments which can determine the values of the nonadiabatic spin torque and the Gilbert damping parameter from the phase of the oscillation with respect to the exciting current.

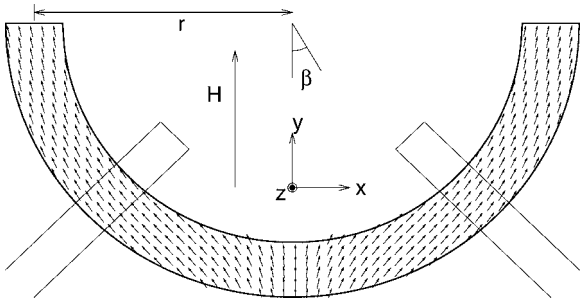

FIG. 1. Scheme of the semicircle nanowire with radius r in a magnetic field H. The static magnetization in the absence of a current is indicated by small arrows. The two rectangles under angles $\beta=\pm 45°$ are the electrical contacts.

II. MODEL

Figure 1 shows a ferromagnetic semicircle nanowire with a domain wall at its bottom placed in an external magnetic field.[37] The wall is excited by an oscillating current flowing between the two contacts.[9]

The magnetization dynamics of a magnetic wire is well described by the Landau-Lifshitz-Gilbert (LLG) equation.[38] In the presence of a spin-polarized current density $\vec{j}$, the interaction between the itinerant electrons and the magnetization $\vec{M}$ leads to an extension of the LLG equation. This extension was derived from a quantum mechanical model by Zhang and Li.[21] Their semiclassical approximation results in the extended LLG equation in Gilbert's form

$$\frac{d\vec{M}}{dt} = -\gamma \vec{M} \times \vec{H}_{\text{eff}} + \frac{\alpha}{M_s}\vec{M} \times \frac{d\vec{M}}{dt} - \frac{b_j}{M_s^2}\vec{M} \times [\vec{M} \times (\vec{j} \cdot \vec{\nabla})\vec{M}] - \xi \frac{b_j}{M_s}\vec{M} \times (\vec{j} \cdot \vec{\nabla})\vec{M}, \tag{1}$$

with the gyromagnetic ratio γ, the Gilbert damping parameter α, the saturation magnetization M_s, and the ratio between exchange relaxation time and spin-flip relaxation time $\xi=\tau_{\text{ex}}/\tau_{\text{sf}}$. The effective magnetic field H_{eff} includes the external as well as the internal fields. In this model the spin current is sensitive to the spatial inhomogeneities of the magnetization with a coupling constant $b_j=\frac{P\mu_B}{eM_s(1+\xi^2)}$ where P denotes the spin polarization of the current and μ_B is the Bohr magneton.

Since the saturation magnetization is constant for a given material at fixed temperature, $\vec{M}$ is perpendicular to $\frac{d\vec{M}}{dt}$ and Eq. (1) can be reformulated to an explicit equation of motion for the magnetization

$$\frac{d\vec{M}}{dt} = -\gamma' \vec{M} \times \vec{H}_{\text{eff}} - \frac{\alpha\gamma'}{M_s}\vec{M} \times (\vec{M} \times \vec{H}_{\text{eff}}) - \frac{b_j'}{M_s^2}(1+\alpha\xi)\vec{M} \times [\vec{M} \times (\vec{j} \cdot \vec{\nabla})\vec{M}] - \frac{b_j'}{M_s}(\xi-\alpha)\vec{M} \times (\vec{j} \cdot \vec{\nabla})\vec{M}, \tag{2}$$

with the abbreviations $\gamma'=\frac{\gamma}{1+\alpha^2}$ and $b_j'=\frac{b_j}{1+\alpha^2}$. This equation is the starting point for the analytical as well as for the numerical calculations presented in the following.

III. ANALYTICAL CALCULATIONS OF THE STRAIGHT WIRE

For the analytical treatment of Eq. (2) we transform the semicircle wire in a homogeneous Zeeman field to a straight wire in a spatially varying field. For this we consider the parallel component of the field. The perpendicular component does not contribute to the domain-wall motion in a *straight* wire and is included in the shape anisotropy. In Sec. IV we will investigate the effect of the perpendicular component of the field on the motion of the domain wall in the *curved* wire and the increase of the exchange energy due to the curvature.

The wire is directed along the x axis and the direction of the magnetization is expressed in a polar spin basis $\vec{M}=M_s(\cos\theta, \sin\theta\cos\phi, \sin\theta\sin\phi)$. In the absence of electric current and external magnetic field the energy of a domain wall within the wire is

$$E = S\int \left[A\left(\frac{\partial\theta(x)}{\partial x}\right)^2 + K\sin^2\theta(x)\right]dx, \tag{3}$$

where θ denotes the angle between the wire axis and the magnetization. A and K denote the exchange and shape anisotropy constants. This functional can be minimized by the well known Néel wall described by the angle

$$\theta = \pi - 2\arctan(e^{(x-X)/\lambda}). \tag{4}$$

The center of the wall is at position X, and the width of the domain wall is $\lambda=\sqrt{A/K}$. From Eq. (4) two expressions

$$\cos\theta = \tanh\left(\frac{x-X}{\lambda}\right), \quad \sin\theta = \frac{1}{\cosh\left(\frac{x-X}{\lambda}\right)} \tag{5}$$

can be derived which will be useful in our further calculations.

In the presence of an external field H_{ext} the demagnetization energy $K_\perp \sin^2\theta\sin^2\phi$ caused by the rotation of the wall around the wire axis can no longer be neglected. We include the external field perpendicular to the wire into the shape anisotropy $K_\perp$. The energy functional in Eq. (3) has to be extended to

$$E = \int \left[K\sin^2\theta + A\left(\frac{\partial\theta}{\partial x}\right)^2 + A\sin^2(\theta)\left(\frac{\partial\phi}{\partial x}\right)^2\right]dV + \int [K_\perp \sin^2\theta\sin^2\phi - \mu_0 M_s H_{\text{ext}}(x)\cos\theta]dV. \tag{6}$$

Here we have restricted ourselves to an external field parallel to the wire. Also the crystalline anisotropy has been neglected.[39] From the energy functional in Eq. (6) we derive the effective magnetic field through the relation $\vec{H}_{\text{eff}}=-\frac{1}{\mu_0}\frac{\delta E}{\delta \vec{M}}$.

We can then write the extended LLG equation (2) in the polar spin basis

$$\dot{\theta} = -\frac{\gamma'}{\mu_0 M_s \sin(\theta)}\frac{\delta E}{\delta \phi} - \frac{\gamma' \alpha}{\mu_0 M_s}\frac{\delta E}{\delta \theta} + b_j'(1+\alpha\xi)\vec{j}\cdot\vec{\nabla}\theta + b_j'(\xi-\alpha)\sin(\theta)\vec{j}\cdot\vec{\nabla}\phi \quad (7)$$

and

$$\dot{\phi}\sin\theta = \frac{\gamma'}{\mu_0 M_s}\frac{\delta E}{\delta \theta} - \frac{\gamma' \alpha}{\mu_0 M_s \sin(\theta)}\frac{\delta E}{\delta \phi} + \sin(\theta) b_j'(1+\alpha\xi)\vec{j}\cdot\vec{\nabla}\phi - b_j'(\xi-\alpha)\vec{j}\cdot\vec{\nabla}\theta. \quad (8)$$

Assuming that the moving wall stays a Néel wall (see Sec. VI) we can describe its motion, following the description of Schryer and Walker[2] by two dynamical variables: the position of its center X and its angle around the wire axis $\phi(x)=\phi$, which is uniform along the wire. With Eqs. (5) and (6) we get from Eqs. (7) and (8)

$$\frac{\sin(\theta)}{\lambda}\dot{X} = -\frac{2K_\perp \gamma'}{\mu_0 M_s}\sin(\theta)\sin(\phi)\cos(\phi) - \alpha\gamma'\sin(\theta)H_{\text{ext}}(x) - \frac{b_\perp'}{\lambda}\sin(\theta)(1+\alpha\xi)j - \frac{2K_\perp \gamma' \alpha}{\mu_0 M_s}\sin(\theta)\cos(\theta)\sin^2(\phi) \quad (9)$$

and

$$\dot{\phi}\sin\theta = \sin(\theta)\gamma' H_{\text{ext}}(x) + \sin(\theta)\frac{b_j'(\xi-\alpha)j}{\lambda} - 2\sin(\theta)\gamma'\alpha K_\perp \sin(\phi)\cos(\phi)\frac{1}{\mu_0 M_s} + \frac{2K_\perp\gamma'}{\mu_0 M_s}\sin(\theta)\cos(\theta)\sin^2(\phi), \quad (10)$$

with the wall width $\lambda = \sqrt{\frac{A}{K+K_\perp \sin^2\phi}} \approx \sqrt{\frac{A}{K}}$.[40] Note that X and ϕ depend on the position x along the wire. In the following we show that a solution consistent with our initial assumptions exists for small exitations.[2] Note that this condition holds for realistic current densities.

Assuming that $H_{\text{ext}}(x)$ varies slowly on the length scale of the domain-wall width $\lambda=\sqrt{A/K}$, $\sin\theta$ is replaced by a δ-function $\pi\lambda\delta(x-X)$ in view of Eq. (5). Also we neglect terms which are nonlinear in ϕ. This approximation holds for angles ϕ smaller than about 10°.

The equations of motion for the domain wall then become

$$\dot{X} = -\lambda 2\gamma' K_\perp \phi\frac{1}{\mu_0 M_s} - \lambda\gamma'\alpha H_{\text{ext}}(X) - b_j'(1+\alpha\xi)j \quad (11)$$

and

$$\dot{\phi} = \gamma' H_{\text{ext}}(X) - 2\gamma'\alpha K_\perp \phi\frac{1}{\mu_0 M_s} + \frac{b_j'(\xi-\alpha)j}{\lambda}. \quad (12)$$

These equations are general equations of motion with a time-dependent current density j. In the limit of a steady current and a homogeneous magnetic field one can calculate the initial velocity of the wall by setting $\phi=0$, the initial condition of the Néel wall. This leads to the initial velocity $\dot{X}_i = -\lambda\gamma'\alpha H_{\text{ext}} - b_j'(1+\alpha\xi)j$ which is exactly the value obtained by Zhang and Li.[21] The terminal velocity $\dot{X}_f = -(\lambda\gamma H_{\text{ext}} + b_j\xi j)/\alpha$ is calculated by setting $\dot{\phi}=0$, i.e., stationary motion. This velocity is also identical to the one calculated by Zhang and Li. Similar relations have recently been found by Dugaev *et al.*[41]

The domain-wall mass is obtained by comparing the ϕ-dependent part of the wall energy in Eq. (6) to the energy E of the domain-wall quasiparticle:

$$\frac{1}{2}m\dot{X}^2 = E = S\int dx K_\perp \sin^2(\theta)\left(\dot{X}\frac{\mu_0 M_s}{\lambda 2\gamma' K_\perp}\right)^2 = \frac{1}{2}\frac{S\mu_0^2 M_s^2}{\lambda\gamma'^2 K_\perp}\dot{X}^2. \quad (13)$$

Here we used

$$\phi = -\dot{X}\frac{\mu_0 M_s}{2\lambda\gamma' K_\perp}, \quad (14)$$

derived from Eq. (11) for stationary motion and in the absence of electric currents and external fields. We arrive at the domain-wall mass

$$m = \frac{S\mu_0^2 M_s^2}{\lambda\gamma'^2 K_\perp}. \quad (15)$$

Note that this result relates the phenomenological domain-wall mass of a Néel wall to the micromagnetic material parameters.

In the case of a curved wire the projection of a uniform external field along the wire is given by $H_{\text{ext}}(x) = H_0\sin(x/r)$. Transferring this to our straight wire model, at small displacements of the domain wall ($X \ll r$) the wall is exposed to the external field $H_{\text{ext}} \approx H_0 X/r$. Then the equations of motion become a system of two coupled linear differential equations of first order:

$$\begin{pmatrix}\dot{X}\\ \dot{\phi}\end{pmatrix} = \gamma'\begin{pmatrix}-\lambda\alpha H_0\frac{1}{r} & -\lambda 2K_\perp\frac{1}{\mu_0 M_s}\\ H_0\frac{1}{r} & -2\alpha K_\perp\frac{1}{\mu_0 M_s}\end{pmatrix}\begin{pmatrix}X\\ \phi\end{pmatrix} + b_j' j\begin{pmatrix}-(1+\alpha\xi)\\ \frac{(\xi-\alpha)}{\lambda}\end{pmatrix}. \quad (16)$$

Except for the nonvanishing first matrix element $-\lambda\alpha H_0/r$ these equations are equivalent to those of a driven harmonic oscillator. For a time-dependent current density of the form $j_0 e^{i\Omega t}$ the general solution

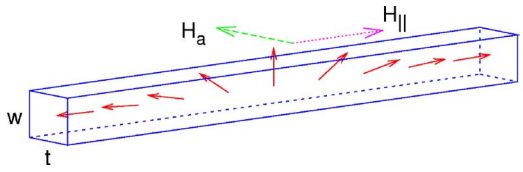

FIG. 2. (Color online) Schematic illustration of the magnetization in the Néel wall (solid red arrows) in a straight wire of width w and thickness t. $H_{\|}$ and H_a are the parallel components of the external field and the anisotropy field, respectively.

$$\begin{pmatrix} X(t) \\ \phi(t) \end{pmatrix} = \begin{pmatrix} X_+ \\ \phi_+ \end{pmatrix} e^{-\Gamma t + i\omega_f t} + \begin{pmatrix} X_- \\ \phi_- \end{pmatrix} e^{-\Gamma t - i\omega_f t} + \frac{1}{\omega_r^2 - \Omega^2 + 2i\Omega\Gamma} \frac{\vec{F}}{m} \tag{17}$$

consists of an exponentially damped starting configuration with the initial conditions described by $X_\pm$ and $\phi_\pm$ and a current-driven oscillation with the driving force $\vec{F}$. The damping constant

$$\Gamma = \alpha\gamma' \left(\frac{\lambda H_0}{2r} + \frac{K_\perp}{\mu_0 M_s} \right) \tag{18}$$

depends on the ratio of applied magnetic field and ring radius. It represents the restoring force acting on the domain wall. This dependence of the damping constant on the restoring force expresses that the damping is spatially dependent. This also leads to a second term in the frequency of the free oscillation,

$$\omega_f = \sqrt{\frac{2\gamma'^2 H_0 \lambda K_\perp}{\mu_0 M_s r} - \alpha^2 \gamma'^2 \left(\frac{K_\perp}{\mu_0 M_s} - \frac{\lambda H_0}{2r} \right)^2}, \tag{19}$$

which is different from Γ. Hence the resonance frequency

$$\omega_r = \sqrt{\omega_f^2 + \Gamma^2} = \sqrt{\frac{2\gamma'^2 H_0 \lambda K_\perp}{\mu_0 M_s r}(1+\alpha^2)} \tag{20}$$

depends explicitly on the Gilbert damping parameter α and differs from the resonance frequency of a normal harmonic oscillator,

$$\omega_0 = \sqrt{\frac{D}{m}} = \sqrt{\frac{2\gamma'^2 H_0 \lambda K_\perp}{\mu_0 M_s r}}, \tag{21}$$

by the factor $\sqrt{1+\alpha^2}$. The constant D is given by $D=F_H/X$ where F_H is the force on the domain wall due to the external magnetic field. The force

$$\vec{F} = -mb_j j_0 e^{i\Omega t} \left(\frac{2\gamma' K_\perp \xi}{\mu_0 M_s} + \frac{1+\alpha\xi}{1+\alpha^2} i\Omega \right) \vec{e}_X - mb_j j_0 e^{i\Omega t} \left(\gamma' H_0 \frac{1}{r} - \frac{\xi - \alpha}{1+\alpha^2} \frac{i\Omega}{\lambda} \right) \vec{e}_\phi, \tag{22}$$

induced by the current, depends on the frequency Ω of the applied current. The terms in Eq. (22) can be understood as direct forces due to the spin torque and the precessions of the magnetization in the external and anisotropy fields depicted in Fig. 2. The terms proportional to $i\Omega$ express the current-induced spin torque. They are the time derivatives of the inhomogenities in Eq. (16). The H_0-dependent term is a result of the precession of the magnetization in the external field which causes a rotation of the wall around the wire axis. The precession in the anisotropy field, described by the $K_\perp$ term in Eq. (22), causes a change of the wall velocity.

Except that the force depends on the frequency Ω of the applied current the result for the domain-wall displacement [Eq. (17)] is equal to the one in a harmonic oscillator. With increasing Ω the force increases and its phase shifts up to 90°. In the absence of a nonadiabatic spin torque ($\xi=0$), current and domain-wall displacement at resonance have opposite sign. In case of a nonadiabatic torque the phase at resonance frequency between the current and the magnetization in the z direction is 90° when the ratio ξ of exchange and spin-flip relaxation time equals the Gilbert damping parameter ($\xi=\alpha$). The phase can be used to find out whether a nonadiabatic spin torque exists and to determine the value of ξ in comparison to the damping parameter α.

The influence of the adiabatic torque on the position of the wall is obtained by setting $\xi=0$ in Eq. (22). The x component of the force $\vec{F}$ due to the adiabatic torque is proportional to the time derivative of the current density. Therefore, the adiabatic torque does not accelerate the wall when the current does not change in time. This explains the observation of Zhang and Li[21] that without a nonadiabatic spin torque a domain wall subjected to a steady current stops moving. In contrast the nonadiabatic contributions to the force are proportional to the current density as well as to its derivative.

In Eq. (17) the starting configuration depends on $\phi_\pm$ and $X_\pm$. The equation that follows from decoupling of Eq. (16),

$$\phi_\pm = \left(\frac{\alpha}{2\lambda} - \frac{\alpha H_0 \mu_0 M_s}{4rK_\perp} \mp i \frac{\omega_f \mu_0 M_s}{2\lambda\gamma' K_\perp} \right) X_\pm, \tag{23}$$

connects $\phi_\pm$ with $X_\pm$. Hence we have two parameters left for our starting configuration as expected for an oscillation.

With the above analytical model—i.e., Eqs. (15) and (17)–(22)—we are able to derive the hitherto phenomenological oscillator model[9] and to express its characteristics by the micromagnetic material parameters. Likewise, the measurement of the domain-wall motion allows the determination of micromagnetic quantities.

IV. CURVED WIRES

For curved wires in a homogeneous magnetic field its component perpendicular to the wire has to be taken into account. Also the change of the magnetization due to the curvature becomes important. To include the perpendicular field we calculate the force on the domain wall as the spatial derivative of its Zeeman energy. The total magnetic moments parallel to the wire,

$$m_{\|} = \int M_s \cos[\theta(x)] dV = -2M_s S X, \tag{24}$$

and perpendicular to the wire,

$$m_\perp = \int M_s \sin[\theta(x)]dV = \pi M_s S\lambda, \tag{25}$$

are volume integrals over its magnetization that are readily calculated using the relations in Eq. (5). Note that $m_\parallel$ is the magnetic moment of an abrupt domain wall. With the magnetic field H_0 in the y direction the Zeeman energy can be written as

$$E_\parallel = \mu_0 M_s H t \int_{r-w/2}^{r+w/2} r' \left[\int_{-\pi/2}^{\beta_0} \sin(\beta) d\beta - \int_{\beta_0}^{\pi/2} \sin(\beta) d\beta \right] dr', \tag{26}$$

where $\beta_0 = \frac{X}{r}$ is the angle of the position of the domain wall (see Fig. 1) and r, w, and t are the radius, the width, and the thickness of the wire. We get

$$E_\parallel = -2\mu_0 M_s S r H \cos(\beta_0) = 2\mu_0 M_s S H Y, \tag{27}$$

with the cross section $S=wt$. One recognizes that the energy is equivalent to the energy of a monopole with magnetic charge $Q_M = 2\mu_0 M_s S$. For small domain-wall displacements we can write the cosine in Eq. (27) as a Taylor series up to second order in X and get

$$E_\parallel \approx -2\mu_0 M_s S r H \left(1 - \frac{X^2}{2r^2}\right). \tag{28}$$

The monopole has been included in the calculations in Sec. III as well as in the calculations of Saitoh *et al.*[9] The perpendicular magnetization contributes to the Zeeman energy by a term

$$E_\perp = -\mu_0 m_\perp H \cos\left(\frac{X}{r}\right) \approx -P_M H \left(1 - \frac{X^2}{2r^2}\right), \tag{29}$$

which can be interpreted as the energy of a magnetic dipole with moment $P_M = \mu_0 \pi M_s S\lambda$. The potential $E = E_\parallel + E_\perp$ is parabolic like for the straight wire.[9,34] However, the resonance frequency is higher. The Zeeman energy of the perpendicular magnetization has previously not been included in the magnetic energy. It gives a correction to the magnetic force on the domain wall,

$$F_x = -\frac{dE}{dX} \approx -\frac{2\mu_0 M_s S H}{r} X - \frac{\pi \mu_0 M_s S \lambda H}{r^2} X = -\frac{Q_M H}{r} X - \frac{P_M H}{r^2} X = -\frac{Q_M}{r} X H \left(1 + \frac{\pi\lambda}{2r}\right). \tag{30}$$

Thus, we include the action of a field component perpendicular to the wire by replacing the field in Eq. (17) by an effective field

$$H_e = H\left(1 + \frac{\pi\lambda}{2r}\right). \tag{31}$$

For example, a ring with a width of 370 nm (Ref. 42) and radius of 500 nm experiences an increase in the effective field of approximately 31%.

We now take into acount the curvature of the wire. With decreasing ring radius the angle between neighboring spins in the domain wall shrinks. This leads to an additional contribution to the exchange energy of the wall when its magnetization points out of the wire plane.

To calculate the new exchange energy we change the spin basis to Cartesian coordinates. To distinguish the spin basis from the basis in space we introduce the coordinates $\chi = \cos\theta$, $\eta = \sin\theta\cos\phi$, and $\zeta = \sin\theta\sin\phi$. Moving along the wire the magnetization performs a rotation in the $-\theta$ direction due to the domain wall as well as a rotation around the ζ axis due to the curvature. For small rotations $\Delta\theta$ and $\Delta\beta$ the Cartesian coordinates are given by

$$\chi = \cos(\Delta\beta)\cos(\theta + \Delta\theta) - \sin(\Delta\beta)\sin(\theta + \Delta\theta)\cos(\phi),$$

$$\eta = \cos(\Delta\beta)\sin(\theta + \Delta\theta)\cos(\phi) + \sin(\Delta\beta)\cos(\theta + \Delta\theta),$$

$$\zeta = \sin(\theta + \Delta\theta)\sin(\phi). \tag{32}$$

The exchange energy density is given by

$$W_{ex} = A\left[\left(\frac{\partial\chi}{\partial x}\right)^2 + \left(\frac{\partial\eta}{\partial x}\right)^2 + \left(\frac{\partial\zeta}{\partial x}\right)^2\right]. \tag{33}$$

From Eq. (32) we obtain

$$W_{ex} = A\left(\frac{\partial\theta}{\partial x}\right)^2 + 2A\frac{\partial\theta}{\partial x}\frac{1}{r}\cos\phi - A\frac{1}{r^2}\sin^2\theta\sin^2\phi + \frac{A}{r^2}. \tag{34}$$

The first term is equal to the exchange energy density of the straight wire. The last term is constant and does not depend on the magnetization. In the approximation for small ϕ the other two terms can be rewritten:

$$\Delta W_{ex} = A\frac{\partial\theta}{\partial x}\frac{1}{r}(2 - \phi^2) - A\left(\frac{\phi}{r}\right)^2 \sin^2\theta. \tag{35}$$

Integration leads to the contribution

$$\int dV \Delta W_{ex} = \left(\frac{AS\pi}{r} - \frac{AS2\lambda}{r^2}\right)\phi^2 - \frac{2AS\pi}{r} \tag{36}$$

of the curvature to the anisotropy energy. The last term is a constant which depends neither on X nor on ϕ. The perpendicular anisotropy energy can be written as

$$\int dV W_{a\perp} = \int dV K_\perp \sin^2\theta \sin^2\phi = K_\perp S 2\lambda \phi^2. \tag{37}$$

Comparing Eqs. (36) and (37) one can see that the additional exchange energy due to the curvature can be included into the perpendicular anisotropy by defining an effective anisotropy constant

$$K_{\perp\text{eff}} = K_\perp + \frac{A\pi}{2\lambda r} - \frac{A}{r^2}. \tag{38}$$

By this equation and Eq. (31) for the effective field we have shown that the modifications result in a higher resonance frequency, higher damping constant, and in a lower domain-wall mass in comparison to the straight wire.

V. NUMERICAL CALCULATIONS

To check the applicability of the approximations made in our analytical model—i.e., the form invariance of the domain wall at small displacements—we have performed micromagnetic simulations. We have modeled current-induced domain-wall oscillations in curved nanowires as described in Sec. II. The current contacts are arranged under an angle of 90° to have sufficient distance to the domain wall as well as to the ends of the wire (see Fig. 1).

We extended the implementation of the Landau-Lifshitz-Gilbert equation in the object-oriented micromagnetic framework[43] (OOMMF) by the additional current-dependent terms of Eq. (2) and implemented Runge-Kutta and Adams-Bashforth-Moulton algorithms of higher order to speed up the calculations. The calculations presented here have been performed using the explicit embedded Runge-Kutta 5(4) algorithm by Cash and Karp.[44] The current density is calculated by locally solving Ohm's law, thus taking the curvature of the wire and the contacts into account. For the spatial discretization a cell size of 1 nm in the x and y directions and 10 nm in the z direction was chosen. Numerical calculations were performed for radii of 45 nm, 55 nm, 65 nm, 70 nm, 85 nm, and 95 nm with different polarized current densities $j_p = jP$. Small radii are chosen so that the corrections from Sec. IV become pronounced. We use the material parameters of Permalloy: i.e., the exchange constant $A = 13 \times 10^{-12}$ J/m and the saturation magnetization $M_s = 8 \times 10^5$ A/m. All wires have a quadratical cross section $S = wt = 100$ nm^2. The applied field in the y direction was chosen to be 125 mT to increase the resonance frequency [see Eq. (20)] and thus to reduce the simulation time necessary for the domain wall to perform several oscillations. Due to the small width of the wire, this high field has virtually no effect on the ground state ($H=0$) of the magnetization. In the ground state we obtain a domain-wall width of $\lambda = 9.25$ nm. The difference in the magnetization orientation θ between the analytical description of the Néel wall and the micromagnetic ground state in the curved wire is less than 5°.

We have determined the eigenmodes of the magnetization in the wire by applying a magnetic δ pulse in the z direction (see Fig. 1), thus exciting all frequencies with equal amplitude. To mimic an applied current, the magnetic field pulse has been chosen to point in the z direction so that the torque of the field points in the same direction as the torque of the applied current [see Eq. (2)]. After this excitation the system performs damped free oscillations. The eigenmodes of the wire are found by spatially resolved discrete Fourier transformation (see Fig. 3).[45,46] The higher harmonics and the standing spin waves in the wire are neglected in the analytical description. The resonance of the ground mode is observed at a frequency of $\Omega = 15.7$ GHz. The higher modes are also indicated in Fig. 3. However, in the following we focus on the ground mode.

We simulated an alternating current with frequencies close to the resonance frequency of the domain wall for different radii r and Gilbert damping parameters α. Figure 4 shows the numerically obtained amplitudes for different radii at fixed $\alpha = 0.05$ and $\xi = 0.01$. For each radius the position and the width of the resonance curve have been fitted to the analytical model, Eq. (17), to determine the parameters $F(r)$, $\omega_r(r)$, and $\Gamma(r)$. Note that all resonance curves are in excellent agreement with the harmonic-oscillator model. The frequencies $\omega_r(r)$ and the damping constants $\Gamma(r)$ have been summarized in Fig. 5 where they are compared to the analytical expressions in Eqs. (18) and (20). The results coincide if we assume $K_{\perp\mathrm{eff}} = K_\perp + \frac{A\pi}{2\lambda r} - \frac{A}{r^2}$ with $K_\perp = 60\,000$ J/m^3 for the perpendicular anisotropy [see Eq. (38)]. The dependence of the resonance frequency ω_r on the radius r according to the phenomenological model of Saitoh *et al.*[9] is also shown. It is visible from Fig. 5 that the analytical model and the phenomenological oscillator model yield the same eigenfre-

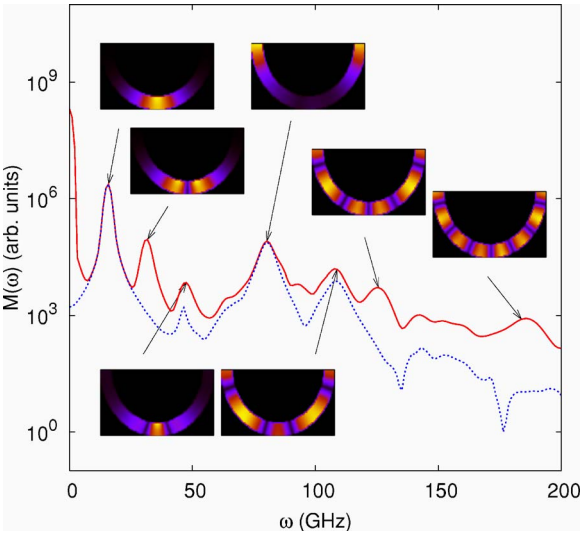

FIG. 3. (Color online) Fourier transform $M(\omega)$ of the simulated magnetization $M_x(t)$ in a curved nanowire with radius $r=45$ nm and Gilbert damping parameter $\alpha=0.05$. The wire is excited with a magnetic δ pulse. The lines show the spatially resolved (solid line) and the integral response (dashed line). The insets show the spatially resolved discrete Fourier transforms for seven selected eigenfrequencies.

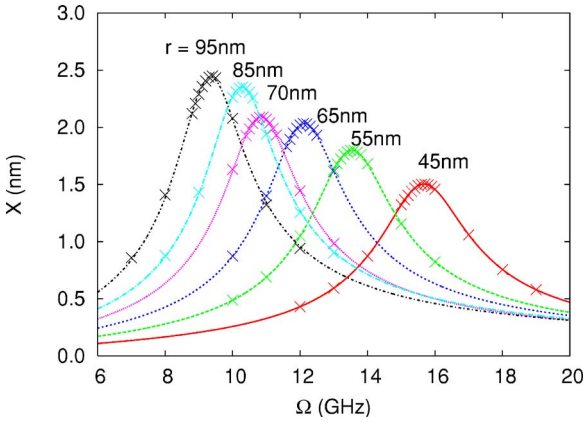

FIG. 4. (Color online) Amplitude of the domain-wall displacement versus frequency of the applied current for different radii r. The Gilbert damping $\alpha=0.05$, the ratio of the exchange and spin-flip relaxation time $\xi=0.01$, and the polarized current density $j_p = 10^{11}$ A/m^2 are fixed. The crosses denote numerical values while the lines are fits with the analytical result of Eq. (17).

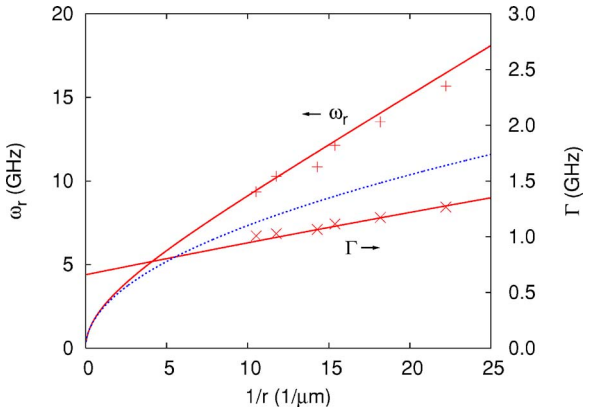

FIG. 5. (Color online) Resonance frequency ω_r and damping constant Γ versus reciprocal ring radius. Shown are the values determined from the fits in Fig. 4 (data points) and the analytical values (solid lines). The dashed line indicates the behavior of the resonance frequency as expected from the phenomenological model of Saitoh *et al.* (Ref. 9)

quencies in the limit of a straight wire ($r \gg 1$ μm). For smaller radii the phenomenological model gives eigenfrequencies which are significantly lower than the ones of the numerical calculations. Our analytical model including the geometrical corrections fits the numerical data very well.

Figures 6 and 7 show the corresponding data for a ring with a radius of 45 nm and different values of the Gilbert damping parameter α. The analytical solutions are calculated with no free fit parameter. While the data points for the damping constant $\Gamma(\alpha)$ coincide with the analytical result, small deviations occur in the resonance frequency $\omega_r(\alpha)$. These deviations can be attributed to the finite cell size in our simulations.

In Figs. 8 and 9 the values for the fit parameter $F(\alpha, r)$ are compared with the analytical result. The analytical values exceed the numerically obtained parameters by up to a factor

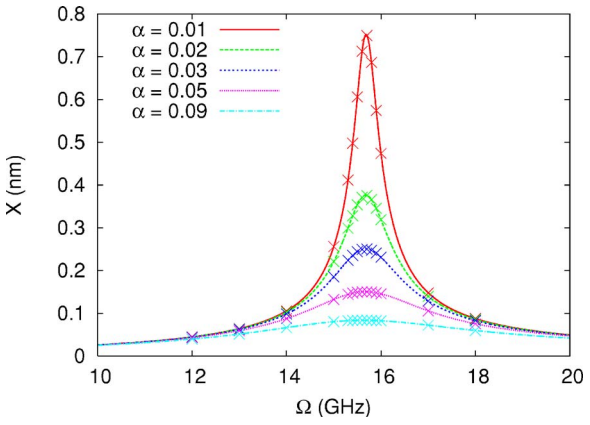

FIG. 6. (Color online) Amplitude of the domain-wall displacement versus frequency of the applied current for different Gilbert damping parameters α. The ring radius r=45 nm, the ratio of the exchange and spin-flip relaxation time ξ=0.01, and the polarized current density $j_p = 10^{10}\mathrm{A/m}^2$ are fixed. The crosses denote numerical values while the lines are fits with the analytical result of Eq. (17).

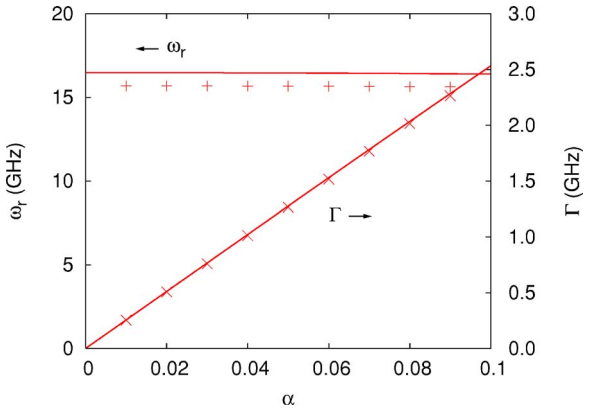

FIG. 7. (Color online) Resonance frequency ω_r and damping constant Γ versus Gilbert damping parameter α. Shown are the values determined from the fits in Fig. 6 (data points) and the analytical values (solid lines).

of 2. This difference has several reasons. In Sec. III we assumed that the ground mode can be described by the motion of the center of the wall X and the magnetization angle ϕ. This neglects spin-wave excitations and higher wall modes. Calculating the mode spectrum excited with a single driving frequency revealed a strong coupling between the ground mode and higher modes. This coupling is enhanced for small radii. Therefore, the force is distributed over several modes, thus decreasing the amplitude of the ground mode. Moreover, in wires with small radii the current distribution is very inhomogeneous with a higher current density at their inner edge. We expect that this leads to an additional deformation of the Néel wall. Another aspect is the finite cell size. In the numerical calculations the curved surface has been approximated with rectangular prisms. The resulting kinks in the wire wall have a measurable effect on the domain-wall motion similar to surface roughness.

VI. RELATION TO EXPERIMENT

In the analytical calculations we assume the linear approximations $\sin(X/r) \approx X/r$ and $\sin\phi \approx \phi$. Nonlinearities

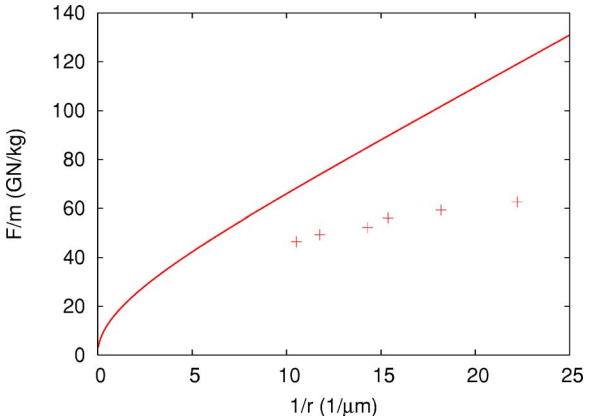

FIG. 8. (Color online) Force per wall mass at the resonance frequency versus reciprocal ring radius. Shown are the numerical values (crosses) and the analytical values (line). The polarized current density is $j_p = 10^{11}\mathrm{A/m}^2$.

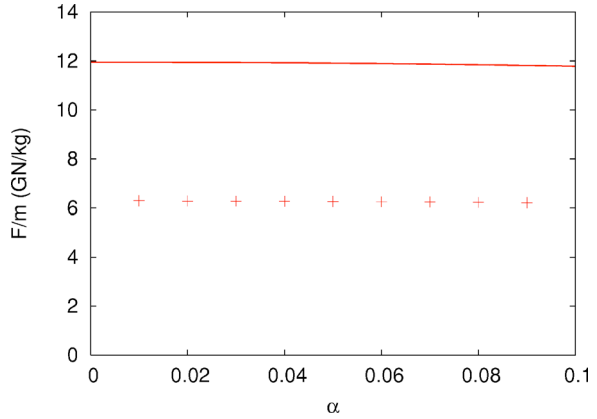

FIG. 9. (Color online) Force per wall mass at the resonance frequency versus Gilbert damping parameter. Shown are the numerical (crosses) and the analytical values (line). The polarized current density is $j_p = 10^{11} \mathrm{A/m^2}$.

cause the deviation of the resonance frequency in Fig. 10 from the analytical form at the current density $j_p = 10^{11}$ A/m^2 and Gilbert damping parameters below 0.05. Note that these nonlinearities are small ($<5\%$). The presented model clearly fails beyond Walker's breakdown.[2] The current densities at which nonlinearities become important strongly depend on the geometry of the wire. Our analytical model allows us to derive them for typical experimental parameters. In the rest of this section we will assume that the damping constant Γ is not field dependent $\left(\frac{\lambda H}{2r} \ll \frac{K_\perp}{\mu_0 M_s}\right)$ and that the squared Gilbert damping parameter is small ($\alpha^2 \ll 1$). These assumptions usually hold in experiments because the domain-wall width λ is small compared to the radius r and the usual values of the damping parameter α are lower than 0.1. We can express all terms in Eq. (22) with the expressions for Γ and ω_r in Eqs. (18) and (20), respectively, when we assume that the ratio of exchange and spin-flip relaxation time ξ is comparable or less than the Gilbert damping parameter α. In the case of a noncritically damped oscillation ($\omega_r > \Gamma$) the oscillation becomes nonlinear if the current density is approximately

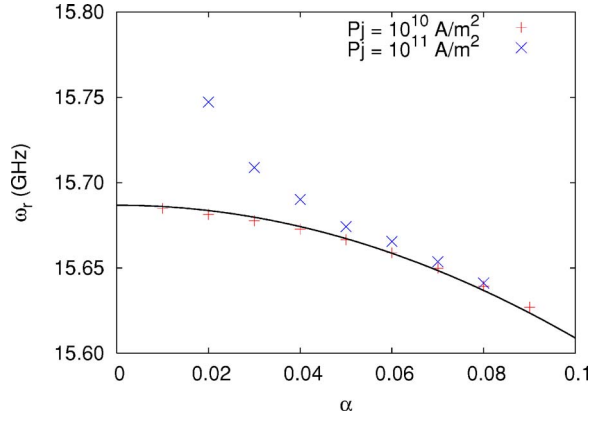

FIG. 10. (Color online) Resonance frequency ω_r versus Gilbert damping parameter α. The data points are the numerical values obtained for a wire with radius 45 nm and two different densities of the polarized current j_p. The line is a fit according to the analytical result $\omega_r = C/\sqrt{1+\alpha^2}$ from Eq. (20) with the fit parameter C.

$$j = \min\left(\frac{\Gamma r}{4b_j}, \frac{\Gamma^2 \lambda}{2\alpha\omega_r b_j}\right). \tag{39}$$

The experimental current densities which Saitoh *et al.*[9] applied on a wire with cross section $S = 3150$ nm^2 and radius $r = 50$ μm are well below this current density. They have determined a domain-wall width $\lambda = 70$ nm, a domain-wall mass $m = (6.55 \pm 0.06) \times 10^{-23}$ kg, and a domain-wall relaxation time $\tau = \frac{1}{2\Gamma} = (1.4 \pm 0.2) \times 10^{-8}$ s. Calculating the demagnetization energy for a straight wire numerically and fitting with the expression for the shape anisotropy $K_\perp \sin^2\theta \sin^2\phi$, we get an anisotropy constant of $K_\perp = 76175$ J/m^3. This yields an effective anisotropy of $K_{\perp \mathrm{eff}} = 76175$ J/m$^3 + \frac{A\pi}{2\lambda r} - \frac{A}{r^2}$. Using Saitoh's experimental parameters we obtain from Eq. (15) a domain-wall mass $m \approx 1.2 \times 10^{-23}$ kg. Tatara and Kohno's approach[18] used in the paper of Saitoh *et al.*[9] delivers exactly the same result.

As mentioned in Sec. 3 the analytical calculations lead to relations between the micromagnetic material parameters and the parameters of the harmonic oscillator. These can be used to experimentally determine the Gilbert damping parameter α from the experimental data. From Eqs. (18), (20), and (15) one can derive the relation

$$\alpha = \frac{2\Gamma \gamma H \lambda}{\omega_r^2 r} = \frac{m \Gamma \gamma \lambda}{\mu_0 M_s S}. \tag{40}$$

With the domain-wall mass and the domain-wall relaxation time of the experiment of Saitoh *et al.* we get a Gilbert damping parameter of $\alpha = 0.0114 \pm 0.0017$. This value agrees quite well with the experimental values of Nibarger *et al.*[47] and Schneider *et al.*[48] which range from 0.008 to 0.017 for film thicknesses between 10 nm and 93 nm.

VII. CONCLUSION

The current-induced motion of a domain wall in thin curved nanowires has been investigated. A harmonic-oscillator model which so far had only been introduced phenomenologically is derived from the LLG equations extended by the spin torque according to Zhang and Li.[21] This derivation relates micromagnetic material parameters to the characteristic quantities describing the oscillating domain wall under the influence of an alternating driving current. It is shown that the dipole moment of the wall and the curvature of the wire have an important influence on the resonance frequency and damping constant of the oscillation. The domain wall can be seen as a quasiparticle in a parabolic potential well which is acted upon by a current-induced force. An important result is that the time derivative of the current density greatly contributes to the force on the domain wall. The phase and magnitude of the force depend on the frequency of the current. The analytical results have been compared to numerical simulations. They agree very well. Our analytical solution suggests new methods to determine material parameters which are otherwise difficult to measure: e.g., the nonadiabatic term of the spin torque can be determined from the phase shift between the applied current and the overall magnetization. Moreover, the Gilbert damping pa-

rameter α and the domain-wall mass m follow from a measurement of the resonance frequency ω_r and the damping constant Γ of the oscillations.

ACKNOWLEDGMENTS

The authors thank S. S. P. Parkin for sharing his results prior to publication. We appreciate fruitful discussions with U. Gummich. Financial support by the Deutsche Forschungsgemeinschaft via SFB 668 "Magnetismus vom Einzelatom zur Nanostruktur" and via Graduiertenkolleg 1286 "Functional metal-semiconductor hybrid systems" is gratefully acknowledged.

[1] A. A. Thiele, J. Appl. Phys. **45**, 377 (1974).
[2] N. L. Schryer and L. R. Walker, J. Appl. Phys. **45**, 5406 (1974).
[3] J. Slonczewski, J. Magn. Magn. Mater. **159**, L1 (1996).
[4] L. Berger, Phys. Rev. B **54**, 9353 (1996).
[5] E. B. Myers, D. C. Ralph, J. A. Katine, R. N. Louie, and R. A. Buhrman, Science **285**, 867 (1999).
[6] J. Grollier, P. Boulenc, V. Cros, A. Hamzi, A. Vaur, A. Fert, and G. Faini, Appl. Phys. Lett. **83**, 509 (2003).
[7] A. Yamaguchi, T. Ono, S. Nasu, K. Miyake, K. Mibu, and T. Shinjo, Phys. Rev. Lett. **92**, 077205 (2004).
[8] H. Koo, C. Krafft, and R. D. Gomez, Appl. Phys. Lett. **81**, 862 (2002).
[9] E. Saitoh, H. Miyajima, T. Yamaoka, and G. Tatara, Nature (London) **432**, 203 (2004).
[10] M. Kläui, C. A. F. Vaz, J. A. C. Bland, W. Wernsdorfer, G. Faini, E. Cambril, and L. J. Heyderman, Appl. Phys. Lett. **83**, 105 (2003).
[11] N. Vernier, D. Allwood, D. Atkinson, M. Cooke, and R. Cowburn, Europhys. Lett. **65**, 526 (2004).
[12] J. A. Katine, F. J. Albert, R. A. Buhrman, E. B. Myers, and D. C. Ralph, Phys. Rev. Lett. **84**, 3149 (2000).
[13] I. N. Krivorotov, N. C. Emley, J. C. Sankey, S. I. Kiselev, D. C. Ralph, and R. A. Buhrman, Science **307**, 228 (2005).
[14] S. S. P. Parkin, US Patent 6,834,005 (2004).
[15] D. A. Allwood, G. Xiong, M. D. Cooke, C. C. Faulkner, D. Atkinson, N. Vernier, and R. P. Cowburn, Science **296**, 2003 (2002).
[16] D. A. Allwood, G. Xiong, C. C. Faulkner, D. Atkinson, D. Petit, and R. P. Cowburn, Science **309**, 1688 (2005).
[17] R. P. Cowburn, Patent Application WO0020040774451A1 (2004).
[18] G. Tatara and H. Kohno, Phys. Rev. Lett. **92**, 086601 (2004).
[19] A. Thiaville, Y. Nakatani, J. Miltat, and Y. Suzuki, Europhys. Lett. **69**, 990 (2005).
[20] X. Waintal and M. Viret, Europhys. Lett. **65**, 427 (2004).
[21] S. Zhang and Z. Li, Phys. Rev. Lett. **93**, 127204 (2004).
[22] Z. Li and S. Zhang, Phys. Rev. B **70**, 024417 (2004).
[23] M. Kläui, C. A. F. Vaz, J. A. C. Bland, W. Wernsdorfer, G. Faini, E. Cambril, L. J. Heyderman, F. Nolting, and U. Rüdiger, Phys. Rev. Lett. **94**, 106601 (2005).
[24] T. Ono, H. Miyajima, K. Shigeto, K. Mibu, N. Hosoito, and T. Shinjo, Science **284**, 468 (1999).
[25] Y. Nakatani, A. Thiaville, and J. Miltat, Nat. Mater. **2**, 521 (2003).
[26] M. Kläui, P.-O. Jubert, R. Allenspach, A. Bischof, J. A. C. Bland, G. Faini, U. Rüdiger, C. A. F. Vaz, L. Vila, and C. Vouille, Phys. Rev. Lett. **95**, 026601 (2005).
[27] A. Yamaguchi, S. Nasu, H. Tanigawa, T. Ono, K. Miyake, K. Mibu, and T. Shinjo, Appl. Phys. Lett. **86**, 012511 (2005).
[28] A. Yamaguchi, T. Ono, S. Nasu, K. Miyake, K. Mibu, and T. Shinjo, Phys. Rev. Lett. **96**, 179904(E) (2006).
[29] J. He, Z. Li, and S. Zhang, Phys. Rev. B **73**, 184408 (2006).
[30] M. Kläui *et al.*, Appl. Phys. Lett. **88**, 232507 (2006).
[31] G. Meier, M. Bolte, R. Eiselt, U. Merkt, B. Krüger, D. Pfannkuche, D. H. Kim, and P. Fischer (unpublished).
[32] D. Atkinson, D. Allwood, G. Xiong, M. D. Cooke, C. C. Faulkner, and R. P. Cowburn, Nat. Mater. **2**, 85 (2003).
[33] M. Hayashi, L. Thomas, Y. B. Bazaliy, C. Rettner, R. Moriya, X. Jiang, and S. S. P. Parkin, Phys. Rev. Lett. **96**, 197207 (2006).
[34] L. Thomas, M. Hayashi, R. Moriya, X. Jiang, C. Rettner, and S. S. P. Parkin, Nature (London) **443**, 197 (2006).
[35] G. Tatara, E. Saitoh, M. Ichimura, and H. Kohno, Appl. Phys. Lett. **86**, 232504 (2005).
[36] N. L. Schryer and L. R. Walker, J. Appl. Phys. **45**, 5406 (1974).
[37] Starting with a high magnetic field the wire is saturated in the y-direction. Reducing the magnetic field to a small offset the system ends up with a domain wall at the bottom of the wire. The wall type depends on the width w and the thickness t of the wire (see Ref. 42). In the present study we choose a small cross section $S=wt=100$ nm^2 with width $w=10$ nm and thickness $t=10$ nm to get a transverse wall.
[38] L. Landau and E. Lifshitz, Phys. Z. Sowjetunion **8**, 153 (1935).
[39] Uniaxial anisotropy can be taken into acount by replacing the anisotropy constants K and $K_{\perp\text{eff}}$ with the new constants K' and $K'_{\perp}$ given by $K'=K+K_y-K_x$ and $K'_{\perp}=K_{\perp\text{eff}}+K_z-K_y$.
[40] Expanding the expression for λ in terms of ϕ shows that the first nonvanishing ϕ-dependent term is quadratic. Since we linearize the equations of motion, we can neglect all nonlinear terms. Then λ is independent of the magnetization angle ϕ.
[41] V. K. Dugaev, V. R. Vieira, P. D. Sacramento, J. Barnaś, M. A. N. Araújo, and J. Berakdar, Phys. Rev. B **74**, 054403 (2006).
[42] Y. Nakatani, A. Thiaville, and J. Miltat, J. Magn. Magn. Mater. **290**, 750 (2005).
[43] OOMMF User's Guide, version 1.0, M. J. Donahue and D. G. Porter, Interagency Report No. NISTIR 6376, National Institute of Standards and Technology, Gaithersburg, MD, 1999 (http://math.nist.gov/oommf/).
[44] J. Cash and A. Karp, ACM Trans. Math. Softw. **16**, 201 (1990).
[45] R. D. McMichael and M. D. Stiles, J. Appl. Phys. **97**, 10J901 (2005).
[46] M. Bolte, G. Meier, and C. Bayer, Phys. Rev. B **73**, 052406 (2006).
[47] J. Nibarger, R. Lopusnik, and T. Silva, Appl. Phys. Lett. **82**, 2112 (2003).
[48] M. Schneider, T. Gerrits, A. Kos, and T. Silva, Appl. Phys. Lett. **87**, 072509 (2005).